Supplementary file for

Detection of Plasmonic Behavior in Colloidal Indium Tin Oxide Films by Impedance Spectroscopy

by Salil M. Joshi, Ning Xia, Rosario A. Gerhardt,* Kenneth C. Littrell, Eric Woods, Yolande Berta, Mengkun Tian and Yong Ding
Georgia Institute of Technology
Atlanta, GA 30332

I. *ITO nanoparticle size analysis and film quality*

Figure S1(a) shows a high-resolution image of the as-synthesized ITO colloidal nanoparticles, taken under an accelerating voltage of 350 kV (JEOL 4000EX Transmission electron microscope). The lattice planes of the ITO nanoparticles are clearly seen in Figure S1(a), indicating that the nanoparticles are crystalline, as has been reported before.[1,2] Quantification of the particle size was also done by small angle neutron scattering using contrast matching[3] by conducting scattering experiments of the same nanoparticles with different solvents as well as varying ratios of hydrogen to deuterium (see Figs. S1(b), (c) and (d)).

Figure S1(b) shows the comparison of the two colloidal solutions examined, which showed an average ITO particle size of ~4.6nm with a fatty acid layer of thickness ranging from 0.5-0.7 nm. More details about the Schultz analysis used to determine the shell thickness can be found at reference 4. Figure S1(c) displays the small angle neutron scattering experiment obtained from colloidal ITO nanoparticle suspensions dispersed in different solvents, while Figure S1(d) depicts the scattering intensity vs Q for a series of H/D ratios in hexane. These curves were used to help with the analysis presented in Figure S1(b).

*contact author: rosario.gerhardt@mse.gatech.edu

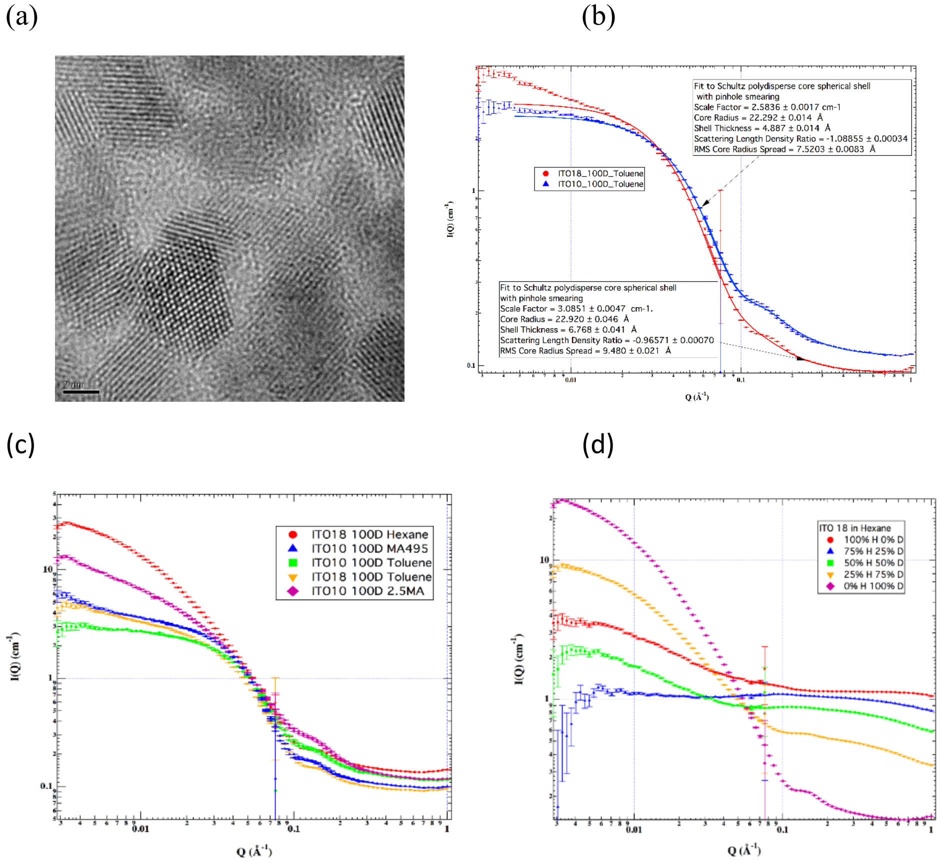

Figure S1. (a) High resolution TEM image of colloidal ITO nanoparticles imaged at 350kV[1].(b) Intensity vs Q from contrast matching small angle scattering analyzed to obtain average ITO particle sizes and their shell thicknes, (c) Intensity vs Q for the same ITO nanoparticles dispersed in different solvents, (d) Contrast matching series for ITO nanoparticles dispersed in hexane as a function of H/D ratio.

II. Analysis of the experimental impedance spectra measured

Since the peak heights for the imaginary impedance vs log frequency presented in Figure 1(g) in the manuscript vary by orders of magnitude, relaxation peaks for all the curves cannot be seen in the Bode plot comparing the imaginary part of impedance. Hence, normalized curves for the imaginary part of impedance are plotted in Figure S2(a) for the purpose of comparison.[5] At least two relaxations and corresponding frequencies of relaxation can be observed for most of the curves. The Z" peaks above the X-axis represent RC relaxation, which is commonly observed in polycrystalline samples. The Z" peaks below the X-axis have appearance similar to those arising from RL relaxations.[6] It can be seen that the frequency of relaxation for both the types of relaxations in Figure 1(d) steadily increases with increase in the annealing temperature. Figure S3(b) shows normalized curves for the imaginary part of the electric modulus for the same data sets as in Figure S3(a). The electric modulus was calculated from the impedance using Equation 1.

$$M^* = j\omega Z^* \qquad \text{Equation 1}$$

It can be seen that the peaks in the Bode plots of normalized Z" that are related to RC relaxations correspond to peaks in the Bode plots of normalized M". This indicates that this relaxation is associated with long-range conductivity and charge transport.[7] In contrast, Z" has an additional time constant due to RL that shows up below the axis and can be seen in Figure S2(a).

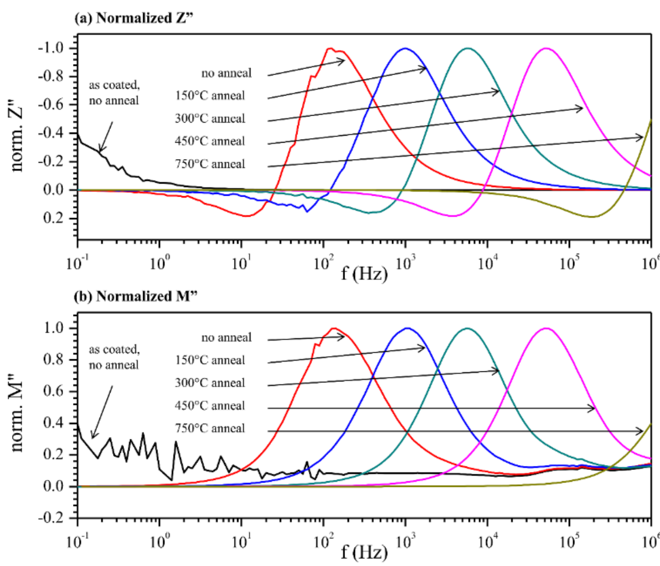

Figure S2: (a) normalized Z", (b) normalized M" vs log frequencycurves showing the presence of two time constants for Z" but only one time constant for M"

Figure S3 shows the variation of the time constants for Z", as determined from the frequency of relaxation as a function of the annealing temperature. It can be seen that the relaxation time constants becomes smaller and smaller with increase in annealing temperature, for both the

RC and RL processes. The frequency range used for impedance spectroscopy was not high enough to observe the RC relaxation in films annealed at 750°C. Hence, that time constant was extrapolated based on the trend; and it is indicated by an unfilled data point in Figure S3. Since these films become more and more conductive with increase in annealing temperature, one might expect the transient charging and discharging at various interfaces within the film. This would naturally lead to smaller relaxation time constants with increasing annealing temperature.

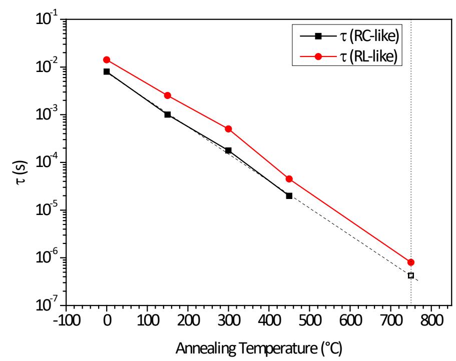

Figure S3: Variation of two relaxation time constants as determined from *Z''* Bode plots shown in Figure 4(a) as a function of annealing temperature (Unfilled point indicates extrapolated point)

III. Equivalent Circuit Data Fitting

Figure S4 show the Bode plots of a representative dataset for the film annealed at 300°C, overlaid with the fitted impedances of the two equivalent circuits proposed in the main article. A good fit can be seen. Some minor mismatch may be observed at the very high frequencies and the very low frequencies. This is commonly observed in experimental data. See the main article for additional explanations.

The various electrical transport processes that may be occurring within the ITO films are shown schematically in **Figure S5**(a)–(e). Some or all of these are thought to occur in the ITO films to various extents during electrical stimulation. The extent to which any or all of these processes may occur depends on the microstructure of the film and the film properties due to the kind of processing the film may have undergone. Schematics of the microstructure of the ITO films for ITO films that did not undergo plasma treatments but did undergo annealing at different temperatures in both air and argon were described in a previous publication[8].

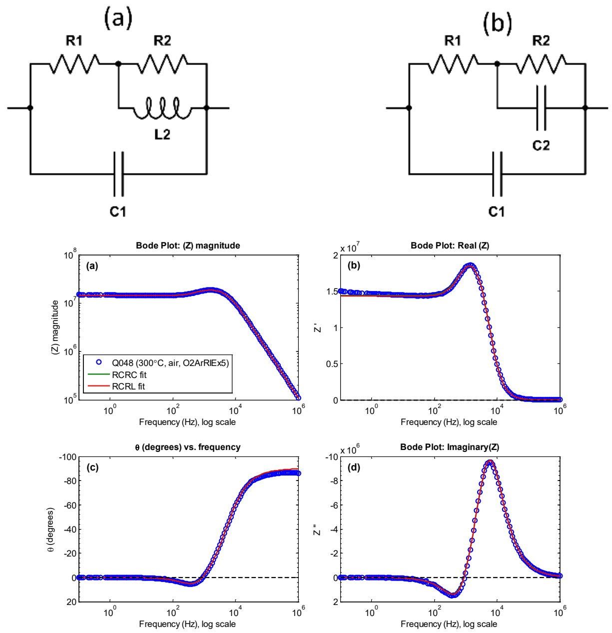

Figure S4: (a) and (b) Circuit elements used to fit the experimental data for all ITO film samples. Two models were evaluated which more or less equally fit the experimental data displayed in (c) where the Bode plots of the averaged impedance spectrum of a colloidal ITO film deposited on fused quartz, annealed at 300°C in air after O_2–Ar RIE x5 plasma treatment. This is overlaid with the corresponding Bode plots of the fitted nested RCRL and RCRC circuits to demonstrate the closeness of fit.

In as-coated films, or those films which have most of the organic coating intact after processing, the microstructure essentially consists of islands of conducting ITO phase dispersed in a non-conducting phase consisting of organics and nano-porosities. Capacitive charge transport, which is schematically shown in **Figure S5**(a), dominates the electrical transport processes in such films.

In addition, there is expected to be a tiny proportion of some leakage current resulting from charge transport across the insulating interfaces. This high interface resistance results in the very large values for R1 in the equivalent circuit discussed above. Since the distance between two nanoparticle surfaces separated by two organic passivating layers (one on each nanoparticle) is very small – estimated to be 3 nm or less (see discussion of synthesized particle size in Section I); there could also be some tunneling component to the charge transport between the coated nanoparticles (shown in **Figure S5**(b)).

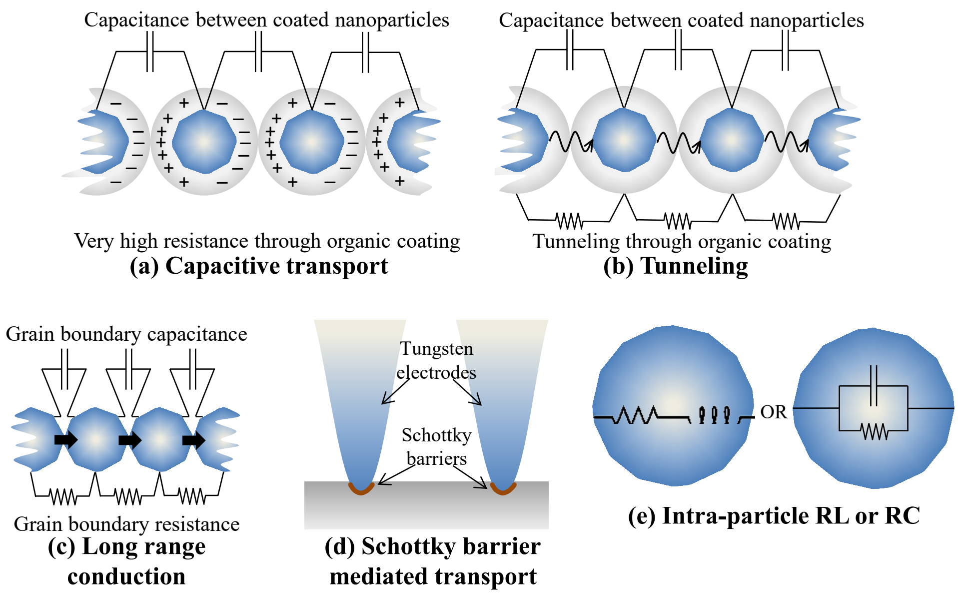

Figure S5: Schematic of some of the various electrical phenomena that may be occurring in the colloidal ITO films: (a) capacitive transport between ITO nanoparticles coated with insulating organics; (b) tunneling across insulating organic coating in the nanoparticles; (c) electron conduction between ITO nanoparticles in electrical contact with each other; (d) Schottky barrier mediated electrical transport between the probes and colloidal ITO film; (e) intra-particle impedance: metallic(resistive-inductive) or resistive-capacitive behavior. From reference 1.

For films with the organic coating completely removed either due to thermal degradation or plasma treatment, the proportion of conductive charge transport will be higher because the nanoparticles are in direct contact with each other. This is shown in **Figure S5**(c). However, with the nanoparticles pretty much only touching each other partially, the quality of electrical contact between them cannot be said to be optimal. As a result, the interface resistance R1 is still moderately high, though lower than in the case of as-coated films. For films that have the organics layer only partially removed, the electrical transport situation is expected to be between the two situations described above. For ITO films which have not only had most of the organics layers removed, but also have had some degree of grain consolidation though necking between grains, the electrical contact between the neighboring particles is improved, resulting in decreased interface resistance R1.

IV. Analysis of the ITO film characteristics

Normalized intensity for ITO thin films measured by X-Ray Diffraction and corresponding Scherrer analysis which indicates that the ITO nanoparticle size essentially does not increase with increasing annealing temperature. Reproduced from Reference 2.

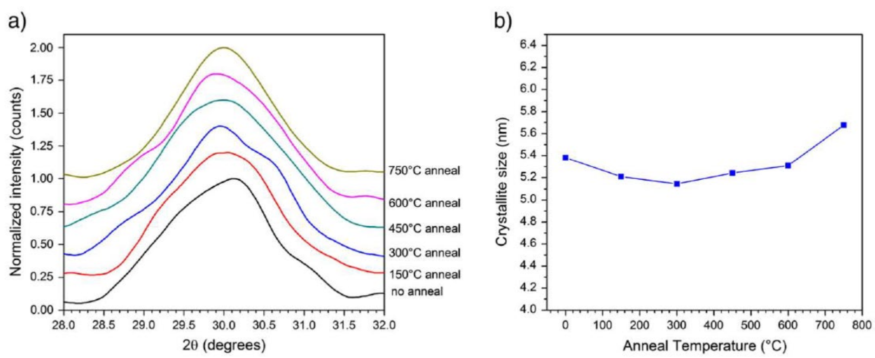

Figure S6. (a) X-ray diffraction scans after background removal and smoothing, of colloidal films annealed in air taken in the vicinity of the strongest peak (222) (b) Crystallite size calculated using the Scherrer relation. From Reference 2.

Figure S7 displays non-contact AFM images (Park Systems XE100E) for ITO films annealed at 150°C, 300°C, 450°C and 750°C which display the presence of interconnected ITO rich regions containing large and small voids that change in size and distribution as the annealing temperature is increased. Figure S8(a) shows an SEM image taken with a Hitachi microscope of the 750°C sample showing the presence of solid and void regions (other samples look very similar). This is reinforced by the TEM images that display the porous regions in S8(b) and a region with isolated particles coated with amorphous polymer in S8(c). Both (b) and (c) were taken with FIB thinned sections. See the main article for more details.

(a) (b) (c) (d)

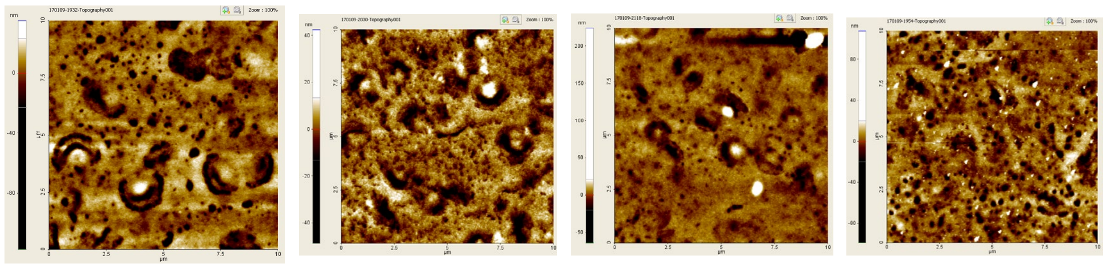

Figure S7. Non-contact AFM images for films annealed at 150°C, 300°C, 450°C and 750°C.

(a) (b) (c)

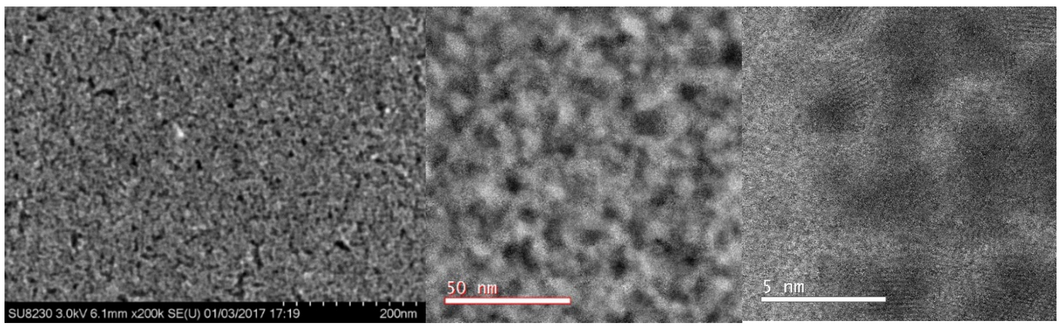

Figure S8. SEM and TEM images of ITO film annealed at 750°C.

The fabricated ITO films are very clear and transparent, as seen in the inset of **Figure S9**. This image shows a chart of the percent transmittance of an as-spin coated ITO film. This measurement was done with a 100% baseline corresponding to an uncoated substrate. It can be seen that the transmittance is very high (~95%) throughout the visible wavelengths (400-700 nm).

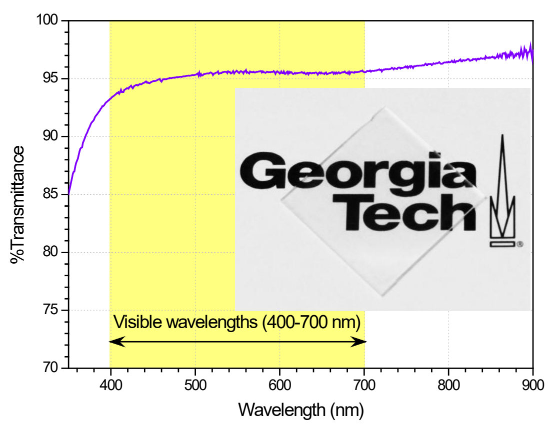

Figure S9: Percent transmittance of an as-coated colloidal ITO film on glass slide (w.r.t uncoated glass slide reference). Inset: As-spin coated colloidal ITO film on a glass substrate. Image was taken of the sample placed on top of the Georgia Tech logo.[1]

References

1. Joshi, Salil M. : Effect of Heat and Plasma Treatments on the Electrical and Optical Properties of Colloidal Indium Tin Oxide Films. PhD dissertation, Georgia Institute of Technology, 2013.
2. Joshi, S.M.; Book, G.W. Book and Gerhardt, R.A, *Thin Solid Films 520:* 2723-2730 (2012)
3. Wignall,G.D.; Littrell,K.C.; Heller, W.T.; Melnichenko,Y.B.; Bailey,K.M. Lynn, G.W.; Myles, D.A.; Urban, V.S.; Buchanan, M.V.; Selbye, D.L.; Butlerf, P.D., The 40 m general purpose small-angle neutron scattering instrument at Oak Ridge National Laboratory. *J. Appl. Cryst.*45, 8898 (2012).
4. Pedersen , J.S. : Analysis of small-angle scattering data from colloids and polymer solutions: modeling and least-squares fitting I, *Adv. Colloid and Interf. Sci.* 70 *,* 171 (1997).
5. Cao, W., Gerhardt, R., & Wachtman, J. : Effect of Sodium Ions on the Dielectric Conductivity of Porous Silica in Humid Environments. *MRS Proceedings, 195,* 471 (1990). *Doi: 10.1557/PROC-195-471, 1990.*
6. Gerhardt, R.A.: Impedance and Dielectric Spectroscopy of Nanoparticulate Films and Composites. *Tech Connect Briefs, Volume: 1*, Nanotechnology 2013: Advanced Materials, CNTs, Particles, Films and Composites. Published: May 12, 2013, pp. 167 – 170 https://briefs.techconnect.org/papers/impedance-and-dielectric-spectroscopy-of-nanoparticulate-films-and-composites/ (ISBN: 978-1-4822-0581-7)
7. Gerhardt, R. A., Impedance and dielectric spectroscopy revisited: Distinguishing localized relaxation from long-range conductivity. *J. Phys. Chem. Solids* 55, 1491 (1994).
8. Joshi, S. M.; Gerhardt, R. A.: Effect of annealing atmosphere (Ar vs. air) and temperature on the electrical and optical properties of spin coated colloidal indium tin oxide films. *J. Mater.Sci.*48, 1465 (2012).